

# Accurate MATLAB Simulink PV System Simulator Based on a Two-Diode Model

Kashif Ishaque\*, Zainal Salam<sup>†</sup>, and Hamed Taheri\*

<sup>†</sup>\* Dept. of Energy Conversion, Faculty of Electrical Engineering, Universiti Teknologi Malaysia, Johor, Malaysia

## Abstract

This paper proposes a MATLAB Simulink simulator for photovoltaic (PV) systems. The main contribution of this work is the utilization of a two-diode model to represent a PV cell. This model is known to have better accuracy at low irradiance levels which allows for a more accurate prediction of PV system performance. To reduce computational time, the input parameters are reduced to four and the values of  $R_p$  and  $R_s$  are estimated by an efficient iteration method. Furthermore, all of the inputs to the simulator are information available on a standard PV module datasheet. The simulator supports large array simulations that can be interfaced with MPPT algorithms and power electronic converters. The accuracy of the simulator is verified by applying the model to five PV modules of different types (multi-crystalline, mono-crystalline, and thin-film) from various manufacturers. It is envisaged that the proposed work can be very useful for PV professionals who require a simple, fast and accurate PV simulator to design their systems.

**Key Words:** Mono-crystalline, Multi-crystalline, PV module, STC, Thin-film

## I. INTRODUCTION

Large and small scale PV power systems have been commercialized in many countries due to their potential long term benefits, generous feed-in tariff schemes and other attractive initiatives provided by various governments to promote sustainable green energy. In PV power generation, due to the high cost of modules, optimal utilization of the available solar energy has to be ensured. This mandates an accurate and reliable simulation of designed PV systems prior to installation.

The most important component that affects the accuracy of a simulation is the PV cell modeling, which primarily involves the estimation of the non-linear  $I$ - $V$  and  $P$ - $V$  characteristics curves. Though impractical, the simplest model is the single diode model i.e. a current source in parallel to a diode [1]-[4]. It only requires three parameters, namely the short-circuit current ( $I_{sc}$ ), the open circuit voltage ( $V_{oc}$ ) and the diode ideality factor ( $a$ ). This model is improved by the inclusion of one series resistance,  $R_s$  [5]-[10], as shown in Fig.1(a). Despite its simplicity, this model exhibits serious deficiencies when subjected to temperature variations. An extension of the model which includes an additional shunt resistance  $R_p$  is shown in Fig.1 (b) [11]-[15]. Although a significant improvement is achieved, this model demands significant computational effort. Furthermore its accuracy deteriorates at low irradiance levels,

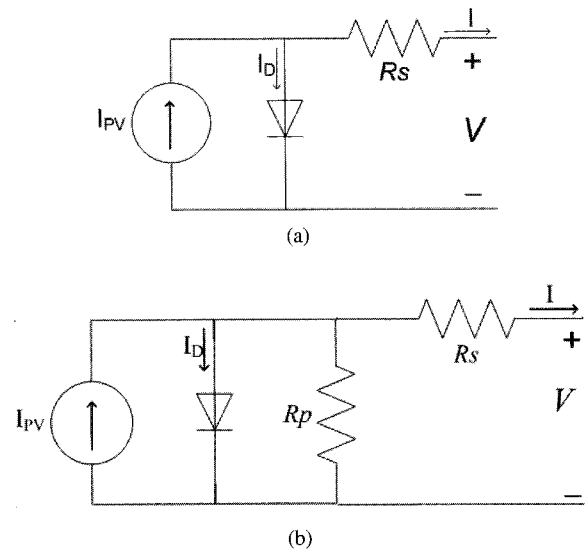


Fig. 1. (a) Solar cell model using single diode model with  $R_s$ . (b) Single diode model with  $R_s$  and  $R_p$ .

especially near  $V_{oc}$ .

The single diode models were based on the assumption that the recombination loss in the depletion region is absent. In a real solar cell, the recombination represents a substantial loss, especially at low voltages. This cannot be adequately modeled using a single diode. Consideration of this loss leads to a more precise model known as the two-diode model [16]. The inclusion of an additional diode increases the parameters. The main challenge now is to estimate the values of all of the model parameters while maintaining a reasonable simulation

Manuscript received Jun. 5, 2010; revised Dec. 9, 2010

<sup>†</sup> Corresponding Author: kashif@fkegraduate.utm.my, zainals@fke.utm.my  
Tel: +607-5536187, Fax: +607-5566272, Universiti Teknologi Malaysia

\* Dept. of Energy Conversion, Faculty of Electrical Engineering, Universiti Teknologi Malaysia, Malaysia

time. Several computational methods have been proposed [17]-[20] but in all of these techniques, new additional coefficients are introduced into the equations, increasing their computational burdens. Furthermore difficulties arise in determining the initial values of the parameters; in some cases heuristic solutions need to be sought. Another approach to describe the two-diode model is by investigating its physical characteristics such as the electron diffusion coefficient, the minority carrier's lifetime, the intrinsic carrier density and other semiconductor parameters [21]-[24]. While these models are useful for understanding the physical behavior of a cell, information about the semiconductors is not always available in commercial PV datasheets. Hence a useful PV simulator using such a model is not feasible because in the majority of the cases the PV designers are not equipped with detailed knowledge of the semiconductor processes.

A complete PV system simulation should fulfill the following criteria: (1) It should be simple and fast but able to accurately predict the  $I$ - $V$  and  $P$ - $V$  characteristic curves, including special conditions such as partial shading. (2) It should be a comprehensive tool which can develop and validate a PV system design inclusive of the power converter and the MPPT control. Although existing software packages like PV-Spice, PV-DesignPro, SolarPro, Pvcad, and PVsyst are available on the market, they are expensive, unnecessarily complex and rarely support the interfacing of the PV arrays with power converters [25].

In this paper a fast and accurate PV system simulator based on the MATLAB-Simulink environment is described. The availability of the simulator in the MATLAB platform is seen as an advantage from the perspective of researchers and practitioners alike because this software has almost become the de-facto standard in various engineering disciplines. An important contribution of this work is the incorporation of a two-diode model as the main engine of the simulator. This model is known to have better accuracy, especially at low irradiance levels. As a result, its application allows for a more accurate prediction of PV system performance especially during partial shading conditions. However, previous researchers have avoided the use of this model in their PV simulators. This is probably due to the significant increased in computational time. Another possible reason why this model has not been used is the insufficient information on certain semiconductor parameters that characterize a specific module. In this work we have devised a computational method that requires only a marginally longer simulation time than the popular single diode model. The input to the simulator is information available in a standard PV module datasheet. In addition, the simulator supports large array simulations that can be interfaced with MPPT algorithms and actual power electronic converters. This allows for performance evaluations when interacting with the other components of a system. The accurateness of the simulator is verified by applying the model to five PV modules of different types (multi-crystalline, mono-crystalline, and thin-film) from various manufacturers. It is envisaged that the proposed work can be very useful for PV professionals who require a simple, fast and accurate PV simulator to design their system.

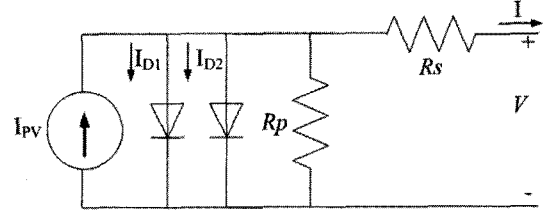


Fig. 2. Two diode model of PV cell.

## II. SIMULATOR DEVELOPMENT

### A. PV Cell Modeling

A more accurate two diode model is depicted in Fig. 2 [16]. Equation (1) describes the output current of the cell:

$$I = I_{PV} - I_{o1} \left[ \exp\left(\frac{V + IR_s}{a_1 V_{T1}}\right) - 1 \right] - I_{o2} \left[ \exp\left(\frac{V + IR_s}{a_2 V_{T2}}\right) - 1 \right] - \left( \frac{V + IR_s}{R_p} \right) \quad (1)$$

where  $I_{o1}$  and  $I_{o2}$  are the reverse saturation currents of diode 1 and diode 2,  $V_{T1}$  and  $V_{T2}$  are the thermal voltages of their respective diodes, and  $a_1$  and  $a_2$  represent the diode ideal constants. The  $I_{o2}$  term in (1), compensates the recombination loss in the depletion region as described in [26].

Although greater accuracy can be achieved using this model, it requires the computation of seven parameters, namely  $I_{PV}$ ,  $I_{o1}$ ,  $I_{o2}$ ,  $R_p$ ,  $R_s$ ,  $a_1$  and  $a_2$ . To simplify this, several researchers assumed that  $a_1 = 1$  and  $a_2 = 2$ . These values are approximations of the Schokley-Read-Hall recombination in the space charge layer of the photodiode [39]. Although this assumption is widely used it is not always true [27]. As discussed in the introduction, many attempts have been made to reduce the computational time of this model. However these attempts appear to be unsatisfactory.

### B. Improved computational method

1) *Simplification of the Saturation Current Equation:* The equation for the PV current as a function of temperature and irradiance can be written as:

$$I_{PV} = (I_{PV\_STC} + K_i \Delta T) \frac{G}{G_{STC}} \quad (2)$$

where  $I_{PV\_STC}$  (in Ampere) is the light generated current under Standard Test Conditions (STC),  $\Delta T = T - T_{STC}$  (in Kelvin,  $T_{STC} = 25^\circ\text{C}$ ),  $G$  is the surface irradiance of the cell and  $G_{STC}$  ( $1000\text{W/m}^2$ ) is the irradiance under STC. The constant  $K_i$  is the short circuit current coefficient, normally provided by the manufacturer. The well known diode saturation current equation [6] is given as:

$$I_0 = I_{0,STC} \left( \frac{T_{STC}}{T} \right)^3 \exp\left[ \frac{qE_g}{ak} \left( \frac{1}{T_{STC}} - \frac{1}{T} \right) \right] \quad (3)$$

where  $E_g$  is the band gap energy of the semiconductor and  $I_{0,STC}$  is the nominal saturation current. An improved equation to describe the saturation current which considers temperature variations is given by [15]:

$$I_0 = \frac{(I_{sc\_STC} + K_i \Delta T)}{\exp[(V_{oc\_STC} + K_v \Delta T)/aV_T] - 1} \quad (4)$$

The constant  $K_V$  is the open circuit voltage coefficient. This value is available from datasheets. To further simplify the model, in this work, both of the reverse saturation currents,  $I_{o1}$  and  $I_{o2}$  are set be to equal in magnitude.

$$I_{o1} = I_{o2} = \frac{(I_{sc\_STC} + K_I \Delta T)}{\exp[(V_{oc\_STC} + K_V \Delta T) / \{(a_1 + a_2) / p\} V_T] - 1}. \quad (5)$$

The equalization simplifies the computation as no iteration is required. As a result, the solution can be obtained analytically. The diode ideal factors  $a_1$  and  $a_2$  represent the diffusion and recombination current components, respectively. In accordance with Shockley's diffusion theory, the diffusion current,  $a_1$  must be unity [16]. The value of  $a_2$ , however, is flexible. Based on the extensive simulations that were carried out, it was found that if  $a_2 \geq 1.2$ , the best match between the proposed model and the practical  $I$ - $V$  curve is obtained. Since  $(a_1 + a_2) / p = 1$  and  $a_1 = 1$ , it follows that the variable  $p$  can be chosen to be  $\geq 2.2$ . The following expression for  $I_{o1}$  and  $I_{o2}$  results in:

$$I_{o1} = I_{o2} = \frac{(I_{sc\_STC} + K_I \Delta T)}{\exp[(V_{oc\_n} + K_V \Delta T) / V_T] - 1}. \quad (6)$$

This generalization can eliminate the ambiguity in selecting the values of  $a_1$  and  $a_2$ . Using (2) and (5), the five parameters of this model can be readily determined, i.e.  $I_{PV}$ ,  $I_{o1}$ ,  $I_{o2}$ ,  $a_1$  and  $a_2$ . Furthermore, the iteration process to compute  $I_{o1}$  and  $I_{o2}$  is avoided, resulting in a reduced computing time.

2) *Determination of the  $R_p$  and  $R_s$  Values:* The remaining two parameters, i.e.  $R_p$  and  $R_s$  are obtained through iteration. Several researchers have estimated these two parameters independently, but the results are unsatisfactory. In this work,  $R_p$  and  $R_s$  are calculated simultaneously, similar to the procedure proposed in [15]. This approach has not been applied to a two-diode model. The idea is to maximize the power point ( $P_{mp}$ ) matching; i.e. to match the calculated peak power ( $P_{mp,C}$ ) and the experimental (from the manufacturer's datasheet) peak power ( $P_{mp,E}$ ) by iteratively increasing the value of  $R_s$  while simultaneously calculating the value of  $R_p$ . From (1) under the maximum power point condition, the expression of  $R_p$  can be rearranged and rewritten as:

$$R_p = \frac{V_{mp}(V_{mp} + I_m R_s)}{[V_{mp}\{I_{PV} - I_{d1} - I_{d2}\} - P_{max,E}]} \quad (7)$$

where

$$I_{d1} = I_{o1} \left[ \exp\left(\frac{V + I R_s}{a_1 V_{T1}}\right) - 1 \right] \quad (8)$$

and

$$I_{d2} = I_{o2} \left[ \exp\left(\frac{V + I R_s}{a_2 V_{T2}}\right) - 1 \right]. \quad (9)$$

The initial conditions for both resistances are given below:

$$R_{so} = 0; \quad R_{po} = \frac{V_{mp}}{I_{scn} - I_{mp}} - \frac{V_{ocn} - V_{mp}}{I_{mp}} \quad (10)$$

Fig. 3 depicts the mechanism of the iteration to obtain the correct  $R_s$  value. Two types of PV modules, Kyocera KC200GT [28] and Solarex MSX-60 [29] were chosen for illustration. In every case,  $R_s$  is increased until  $P_{max,C}$  becomes exactly equal to  $P_{max,E}$ . Meanwhile, for each iteration, the value of  $R_p$  is calculated simultaneously using (7).

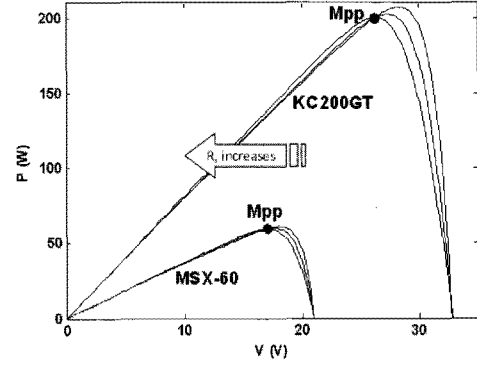


Fig. 3. Matching  $P$ - $V$  curves methodology for three PV modules.

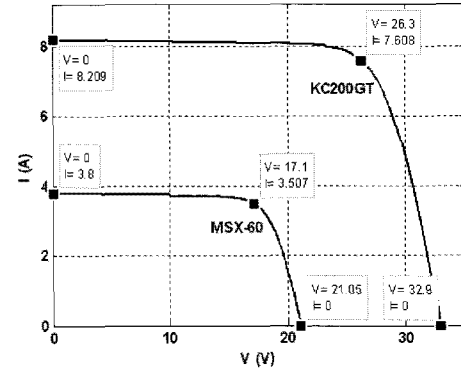


Fig. 4. Matching  $I$ - $V$  curves for KC200GT and MSX-60 modules.

The final matched  $I$ - $V$  curves for the two PV modules are shown in Fig. 4. As can be observed the three important points, namely  $I_{sc}$ ,  $P_{mp}$  ( $V_{mp}$ ,  $I_{mp}$ ) and  $V_{oc}$  strongly agree with the manufacturer data. With the availability of all seven parameters, the output current of the cell can now be determined using the standard Newton-Raphson method. The flowchart that describes the  $P_{mp}$  matching algorithm is given in Fig. 5.

### C. Large Array Simulation

In a typical installation of a large PV power generation system, the modules are configured in a series parallel structure (i.e.  $N_{ss} \times N_{pp}$  modules), as depicted in Fig. 6. To handle such cases, the output current equation given in (11) has to be modified as follows:

$$I = I_{PV} N_{pp} - I_{o1} N_{pp} \left[ \exp\left(\frac{V + I R_s \left(\frac{N_{ss}}{N_{pp}}\right)}{a_1 V_T N_{ss}}\right) - 1 \right] - I_{o2} N_{pp} \left[ \exp\left(\frac{V + I R_s \left(\frac{N_{ss}}{N_{pp}}\right)}{a_2 V_T N_{ss}}\right) - 1 \right] - \left( \frac{V + I R_s \left(\frac{N_{ss}}{N_{pp}}\right)}{R_p \left(\frac{N_{ss}}{N_{pp}}\right)} \right) \quad (11)$$

where  $I_{PV}$ ,  $I_{o1}$ ,  $I_{o2}$ ,  $R_p$ ,  $R_s$ ,  $a_1$ ,  $a_2$  are the parameters of the individual modules.

Fig. 7 shows a building block of a PV array for any number of series parallel connections. The inputs for a two diode model are designed as a template shown in Fig. 8 (a). All of the parameters for the inputs are available from the manufacture's

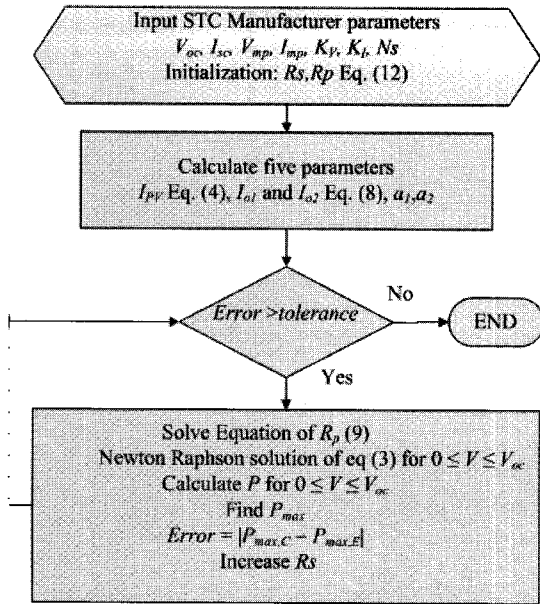


Fig. 5. Matching Algorithm.

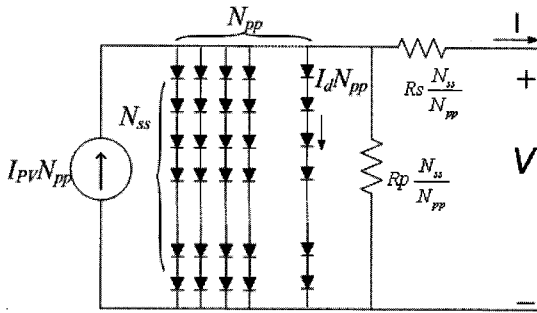


Fig. 6. Series parallel combination in PV array.

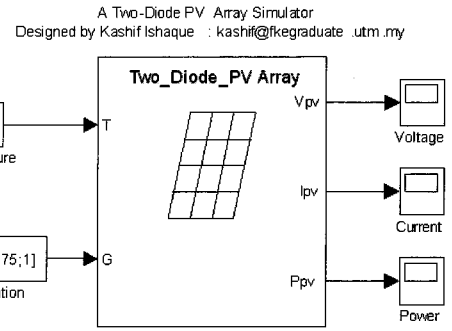


Fig. 7. PV simulator Block in Simulink.

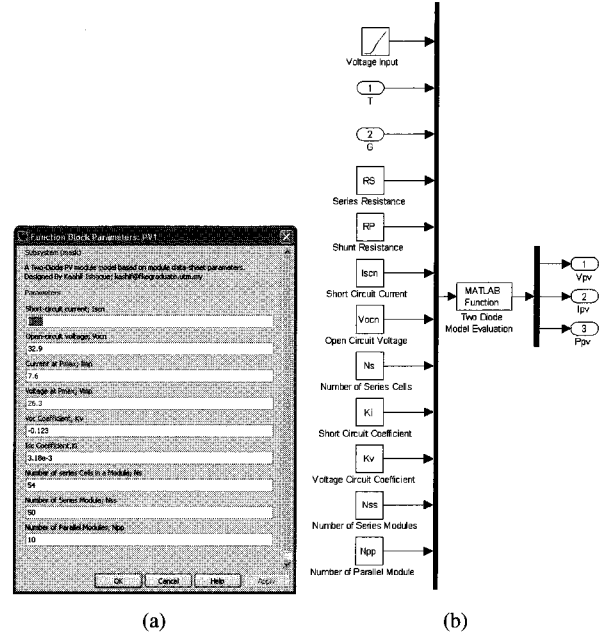


Fig. 8. (a) Input parameter window. (b) mask implementation of PV simulator.

datasheet. A mask implementation two diode PV simulator is shown in Fig. 8 (b).

### III. RESULTS AND DISCUSSION

#### A. Verification of the Two Diode Model

The two diode model described in this paper is validated by the measured parameters of selected PV modules. Five modules of different brands/models are utilized for verification; these include the multi- and mono-crystalline as well as the thin-film types. The specifications of the modules are summarized in Table I. The computational results are compared with the  $R_s$  [6] and  $R_p$  [15] models. Note that these two models are shown in Figs. 1(a) and (b), respectively.

Table II shows the parameters of the proposed two-diode model. Although it has more variables, the actual number of parameters to be computed is only four because  $I_{o1} = I_{o1}$  while  $a_1$  and  $a_2$  can be chosen arbitrarily from (5).

Fig. 9 shows the  $I$ - $V$  curves for a KC200GT module (single), for different levels of irradiation (per unit quantity: Sun=1 equivalent to 1000W/m<sup>2</sup>). The calculated values from the proposed two-diode and  $R_p$ -models are evaluated against the measured data from the manufacturer's datasheet. Comparison with the  $R_s$ -model is not included to avoid overcrowding of the plot. However, the results for the  $R_s$ -model will be analyzed later in the performance evaluation of the three models.

The proposed two-diode model and the  $R_p$ -model exhibit similar results under STC. This is to be expected because both models use similar maximum power matching algorithms to evaluate the model parameters under STC. However, as irradiance gets lower, more accurate results are obtained from the two-diode model, especially in the vicinity of the open circuit voltage. At  $V_{oc}$ , the  $R_p$ -model shows a departure from the experimental data, suggesting that the  $R_p$ -model is inadequate when dealing with low irradiance levels. This is envisaged to have significant implications during periods of partial shading.

The performance of the models when subjected to temperature variations is considered next. All of measurements are conducted under the STC irradiance of 1000W/m<sup>2</sup>. The proposed model is compared with the  $R_s$ -model. This comparison was specifically chosen to highlight the significant problems with the  $R_s$ -model when subjected to temperature variations. The  $R_p$ -model is not shown for the sake of simplicity, but it will be included later in an analysis that compares all three models together. Two modules are tested, namely the KC200GT and the MSX-60. As can be seen in Figs. 10 and 11, respectively, the  $I$ - $V$  curves computed by the two-diode model accurately match the experimental data for all

TABLE I  
TABLE ISTC SPECIFICATIONS FOR THE THREE MODULES USED IN THE EXPERIMENTS

Parameter	BP Solar MSX-60	Multi-Crystalline Kyocera KG200GT	Shell S36	Mono-Crystalline Shell SP-70	Thin-Film Shell ST40
$I_{sc}$	3.8 A	8.21 A	2.3 A	4.7 A	2.68 A
$V_{oc}$	21.1 V	32.9 V	21.4 V	21.4 V	23.3 V
$I_{mp}$	3.5 A	7.61 A	2.18 A	4.25 A	2.41 A
$V_{mp}$	17.1 V	26.3 V	16.5 V	16.5 V	16.6 V
$K_v$	-80 mV/°C	-123 mV/°C	-76 mV/°C	-76 mV/°C	-100 mV/°C
$K_i$	3 mA/°C	3.18 mA/°C	1 mA/°C	2 mA/°C	0.35 mA/°C
$N_s$	36	54	36	36	36

TABLE II  
PARAMETERS FOR THE PROPOSED TWO-DIODE MODEL

Parameter	BP Solar MSX-60	Multi-Crystalline Kyocera KG200GT	Shell S36	Mono-Crystalline Shell SP-70	Thin-Film Shell ST40
$I_{sc}$	3.8 A	8.21 A	2.3 A	4.7 A	2.68 A
$V_{oc}$	21.1 V	32.9 V	21.4 V	21.4 V	23.3 V
$I_{mp}$	3.5 A	7.61 A	2.16 A	4.24 A	2.41 A
$V_{mp}$	17.1 V	26.3 V	16.7 V	16.5 V	16.6 V
$I_{o1} = I_{o2}$	$4.704 \times 10^{-10}$ A	$4.218 \times 10^{-10}$ A	$2.059 \times 10^{-10}$ A	$4.206 \times 10^{-10}$ A	$3.07 \times 10^{-11}$ A
$I_{PV}$	3.80 A	8.21 A	2.3 A	4.7 A	2.68 A
$R_p$	176.4 $\Omega$	160.5 $\Omega$	806.4 $\Omega$	91 $\Omega$	211.7 $\Omega$
$R_s$	0.35 $\Omega$	0.32 $\Omega$	0.89 $\Omega$	0.51 $\Omega$	1.76 $\Omega$

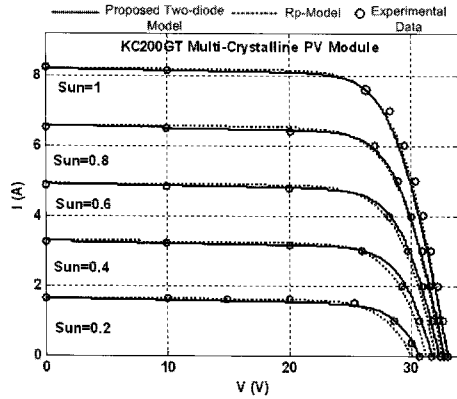


Fig. 9.  $I$ - $V$  curves of  $R_p$ -Model and proposed two-diode model of the KC200GT PV module for several Irradiance levels.

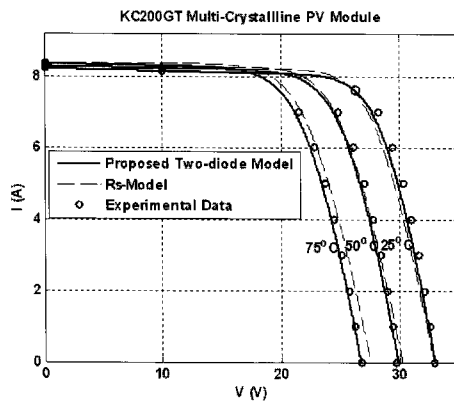


Fig. 10.  $I$ - $V$  curves of  $R_s$  and proposed two-diode model of the KC200GT PV module for several temperature levels.

temperature conditions. In contrast, at higher temperature, the results from the  $R_s$ -model deviate from the measured values quite significantly.

Fig. 12 shows an analyses of the relative error of  $V_{oc}$  and the maximum power point  $P_{mp}$  for a KC200GT module at

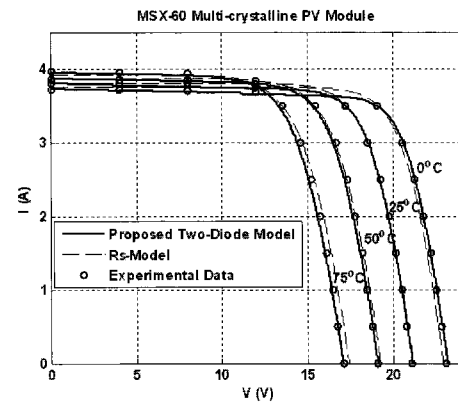


Fig. 11.  $I$ - $V$  curves of  $R_s$  and proposed two-diode model of the MSX 60 PV module for several temperature levels @  $1\text{KW/m}^2$ .

different irradiance levels. The temperature is set to STC. The relative error is defined as the difference between the simulated and the measured  $V_{oc}$  and  $P_{mp}$  values. The difference is then divided by the measured value. As can be seen, under the STC irradiance level, there is a very small difference in the  $V_{oc}$  values among the three models. However as the irradiance is reduced, significant deviations are observed with the  $R_s$  and  $R_p$ -models. Similar results can be seen for the  $P_{mp}$ . On the other hand, the proposed two-diode model accurately calculates  $P_{mp}$  under all irradiance levels.

Fig. 13 shows the performance of the three models when subjected to variations in module temperature. The irradiance is set to STC. There is no significant difference between the  $R_p$  and the two-diode models. However the  $R_s$  model exhibits poor performance in both  $V_{oc}$  and  $P_{mp}$  calculations.

To show the effectiveness of the models for different silicon technologies, comparisons between a S36 (mono-crystalline), a SP70 (multi-crystalline), and a ST40 (thin-film) are carried out. All of these modules were manufactured by Shell [30]. For this test, the irradiance is maintained constant at

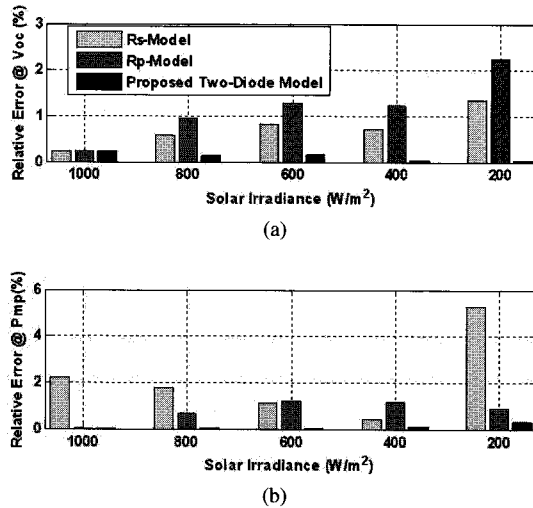


Fig. 12. Relative error for  $V_{oc}$  and  $P_{mp}$ , for  $R_s$ ,  $R_p$  and the proposed two-diode model for KC200GT PV module.

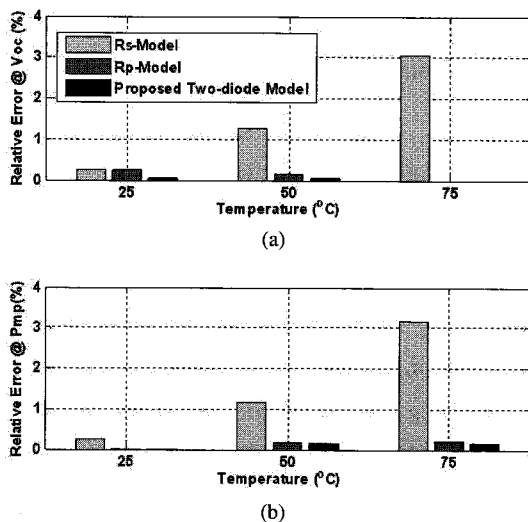


Fig. 13. Relative error for  $V_{oc}$  and  $P_{mp}$ , for  $R_s$ ,  $R_p$  and the proposed two-diode model for KC200GT PV module.

STC. Fig. 14 shows the relative error in  $P_{mp}$  for a wide variation in temperature ( $-25^{\circ}C$  to  $+50^{\circ}C$ ). From the data, it can be concluded that more accurate results are obtained from the two-diode model for all of the silicon technologies. Furthermore, it can be seen that using the  $R_s$ -model results in considerably more errors in the calculation of  $V_{mp}$  and  $P_{mp}$ . This is particularly severe for the thin film technology.

Fig. 15 depicts a comparison of all three modeling techniques when the irradiance is varied from 1000 to  $200 W/m^2$ . A temperature of  $25^{\circ}C$  is maintained in these analyses. As can be seen, better results are obtained with the proposed two-diode model. As expected, the  $R_s$ -model shows a significant variation with the ST40 PV module.

The extensive experimental verification above proves that the two diode model is superior to the  $R_s$  and  $R_p$  single diode models. This justifies its usage in the proposed simulator.

### B. Large System Simulation

The simulator can be used to simulate a large PV array configuration by simply defining the inputs  $N_{ss}$  and  $N_{pp}$  to

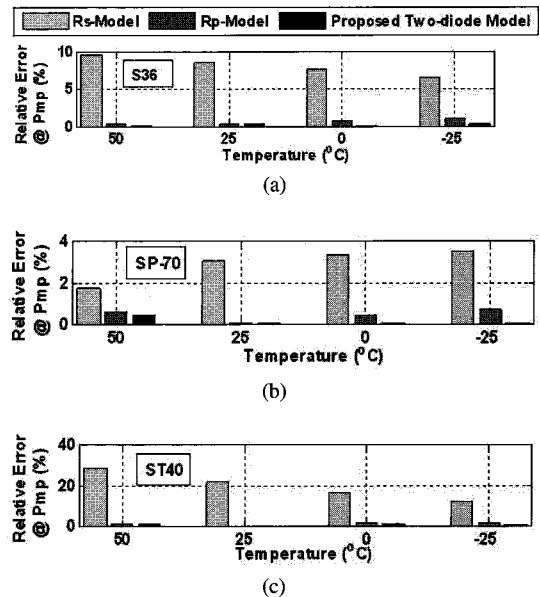


Fig. 14. Relative error for  $P_{mp}$  of  $R_s$ ,  $R_p$  and the proposed two-diode model for temperature variation. (a) S36. (b) SP70 (c) ST40.

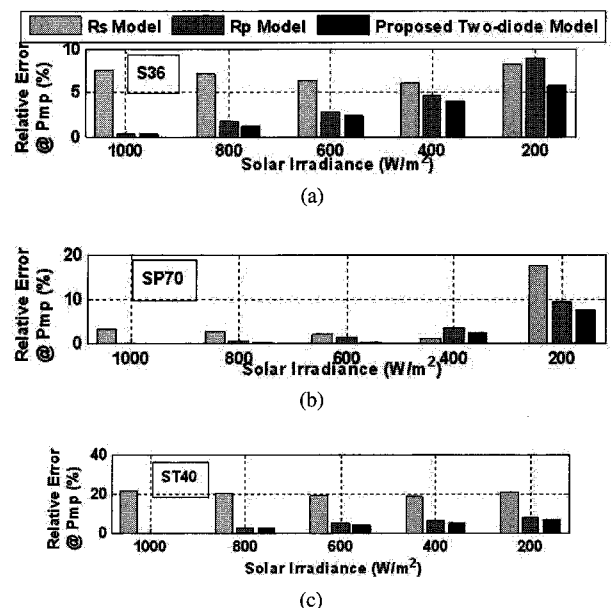


Fig. 15. Relative error for  $P_{mp}$  of  $R_s$ ,  $R_p$  and the proposed two-diode model for irradiance variation. (a) S36. (b) SP70. (c) ST40.

be the number of modules in series and parallel, respectively. Figs. 16 (a) and (b) show the  $I$ - $V$  and  $P$ - $V$  curves generated by the simulator for a  $30 \times 10$  array using KC200GT modules at different irradiance levels. The effects of temperature variations are shown in Figs. 17 (a) and (b). As can be seen, the shapes of the  $I$ - $V$  curves are exactly equivalent to the single module curves shown in Figs. 9 and 10. The current, voltage and power are correctly scaled according to the array configuration. It is worth noting that the simulation time is independent of the array configuration, i.e. it makes no differences in terms of computation time, for any number of series and parallel connected modules.

Due to partial shading or module mismatch, there exists the possibility of multiple local maxima instead of a single  $M_{pp}$ . A PV simulator should be capable of handling the effects of

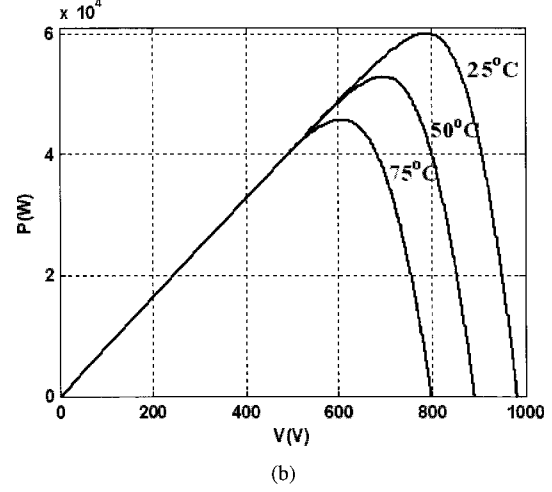
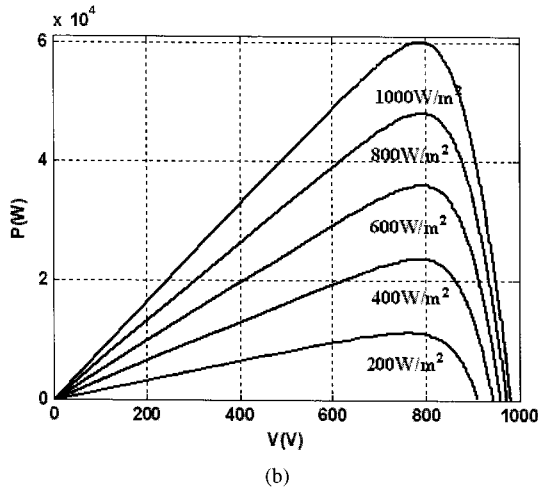
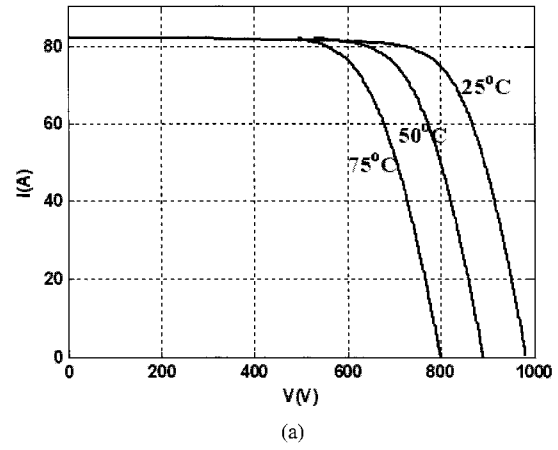
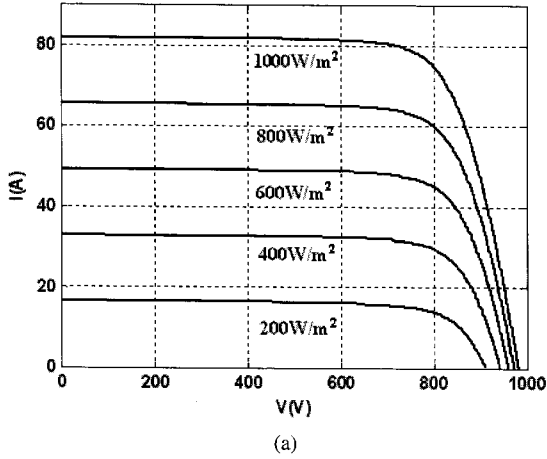


Fig. 16. (a)  $I$ - $V$  curves. (b)  $P$ - $V$  curves for KC200GT in  $50 \times 10$  configuration for different irradiation levels from PV simulator.

Fig. 17. (a)  $I$ - $V$  curves. (b)  $P$ - $V$  curves for KC200GT in  $50 \times 10$  configuration for different temperature levels from PV simulator.

such events. Fig. 18 shows an application of the simulator for a typical partial shading condition. In this example, three shading patterns, i.e.  $G = 1$ ,  $G = 0.75$  and  $G = 0.5$  are applied to the group of modules A, B, and C. Fig. 19 (a) and (b) show the resulting  $I$ - $V$  and  $P$ - $V$  curves for the above shading patterns.

### C. Simulation with Converter and Controller

The capability of the simulator to interface with power electronics converters is illustrate in Fig. 20, in which the simulation of a grid connected PV system involving a boost-type dc-dc converter (with a MPPT controller) and an inverter is carried out. The PV modules are KC2000GT configured in a  $6 \times 2$  array. The boost converter and inverter are designed using an averaging model [31]. For the boost converter, an input series winding resistance of  $0.5 \Omega$  and an output current (source) of  $30 \text{ mA}$  are used to model the conduction and switching losses, respectively. In the same manner, an output series winding resistance of  $0.8 \Omega$  and an output current source of  $40 \text{ mA}$  are used in the inverter to model the conduction and switching losses. A DC link capacitor ( $500 \mu\text{F}$ ) provides the energy storage necessary to balance the instantaneous power delivered to the grid. The capacitor value is calculated

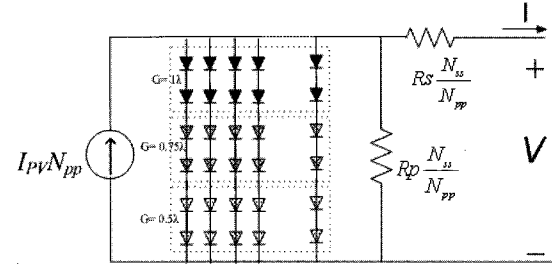


Fig. 18. A PV array illustration for the partial shading condition ( $\lambda=1000 \text{ W/m}^2$ ).

based on an 8% ripple in the  $V_{DC}$ . In the steady-state condition,  $I_{RMSref}$  is adjusted by the current controller to equalize  $V_{DC} = V_{DCref}$ . The error signal then goes to zero and the average power  $P_{ac}$  delivered to the AC grid matches the power generated by the PV array. The MPPT controller utilizes a conventional perturbation and observe (P&O) algorithm. The results of the MPPT controller actions are shown in Fig. 21.

As can be seen in Fig. 21 (a)-(c), until  $t = 0.05 \text{ s}$ , at which point shading occurs, the MPPT controller calculates the correct  $V_{mp}$  voltage ( $26.3 \times 6 \cong 157.8 \text{ V}$ ) and  $I_{mp}$  current ( $7.6 \times 2 \cong 15.2 \text{ A}$ ), respectively, corresponding to the maximum power point. Due to shading of the PV array (at  $t = 0.05 \text{ s}$ ), the conventional P&O algorithm traps the local maximum.

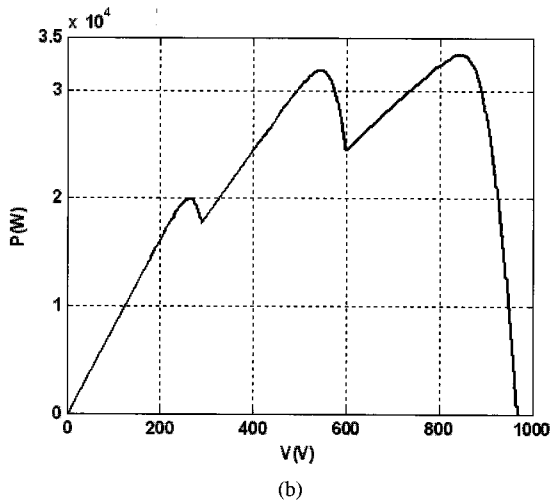
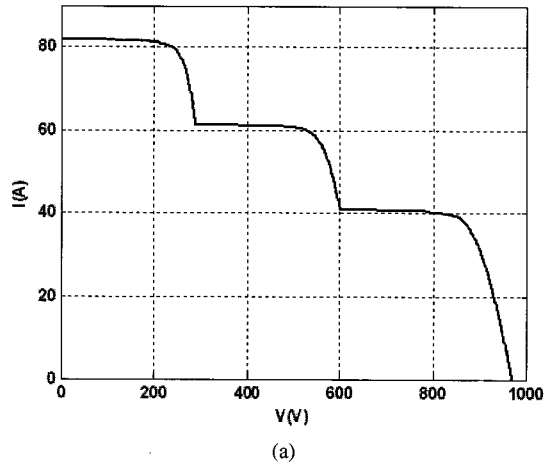


Fig. 19. (a)-(b)  $I$ - $V$  and  $P$ - $V$  characteristics for the shading pattern of figure 18.

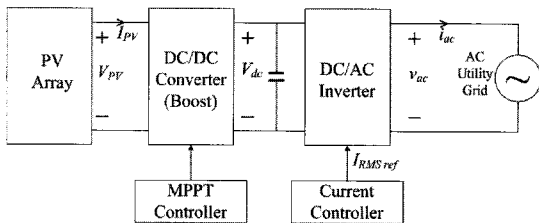


Fig. 20. Grid connected system interfacing with PV simulator.

This condition leads to a decrease in the output voltage of the boost converter, as shown in Fig. 22 (a). Moreover, the AC output power is almost equal to the input power as shown in Fig. 22(c). The expected 120Hz ripple (twice the mains frequency) at the output of the Boost converter is also evident. This exercise proves the accurateness of the simulator.

#### IV. CONCLUSIONS

In this paper, a MATLAB Simulink PV system simulator based on an improved two-diode model is proposed. To reduce the computational time, the input parameters are reduced to four and the values of  $R_p$  and  $R_s$  are estimated by an efficient iteration method. Furthermore the inputs to the simulator are information available on standard PV module datasheets. The simulator supports large array simulations that can be

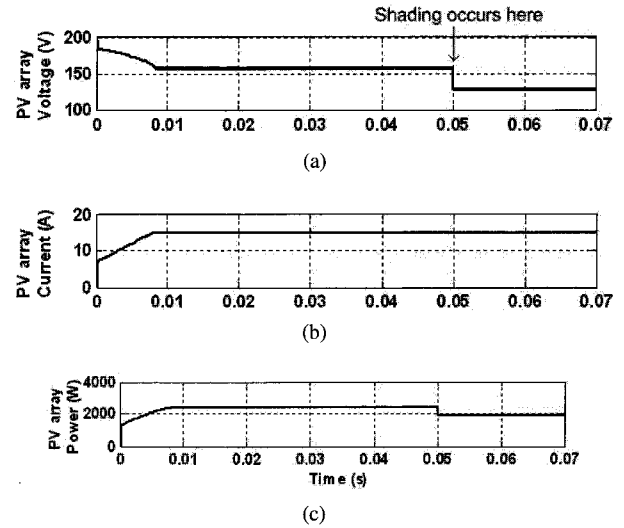


Fig. 21. (a)-(c) Output voltage, current, and output power from the PV array using P&O algorithm.

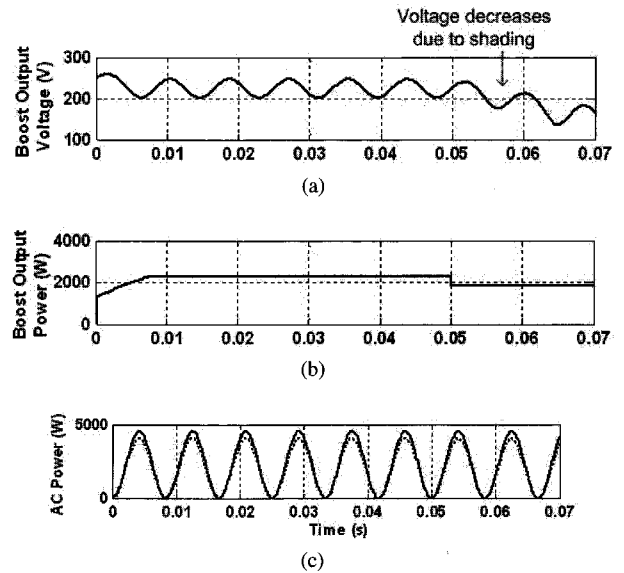


Fig. 22. (a)-(b) Output voltage and output power from the boost converter. (c) AC input (solid) and output power (dotted).

interfaced with MPPT algorithms and actual power electronic converters. The accurateness of the simulator is verified with five PV modules of different types (multi-crystalline, mono-crystalline and thin-film) from various manufacturers. It is observed that the two-diode model is superior to the  $R_p$  and  $R_s$  models. Furthermore, a complete grid connected PV system, together with power converters and controllers is simulated. The results are found to be in close agreement with the theoretical predictions.

#### ACKNOWLEDGMENT

The authors would like to thank the Universiti Teknologi Malaysia for providing the facilities and a research grant to conduct this research.

#### REFERENCES

- [1] M. C. Glass, "Improved solar array power point model with SPICE realization," in *Proc. IECEC*, Vol. 1, pp. 286–291, Aug. 1996.

- [2] Y. T. Tan, D. S. Kirschen, and N. Jenkins, "A model of PV generation suitable for stability analysis," *IEEE Trans. Energy Convers.*, Vol. 19, No. 4, pp. 748–755, Dec. 2004.
- [3] A. Kajihara and A. T. Harakawa, "Model of photovoltaic cell circuits under partial shading," in *Proc. ICIT*, pp. 866–870, 2005.
- [4] N. D. Benavides and P. L. Chapman, "Modeling the effect of voltage ripple on the power output of photovoltaic modules," *IEEE Trans. Ind. Electron.*, Vol. 55, No. 7, pp. 2638–2643, Jul. 2008.
- [5] W. Xiao, W. G. Dunford, and A. Capel, "A novel modeling method for photovoltaic cells," in *Proc. PESC*, Vol. 3, pp. 1950–1956, 2004.
- [6] G. Walker, "Evaluating MPPT converter topologies using a matlab PV model," *J. Elect. Electron. Eng.*, Vol. 21, No. 1, pp. 45–55, 2001.
- [7] F. González-Longatt, *Model of photovoltaic module in MatlabTM*, II CIBELEC, 2005.
- [8] N. Celik and N. Acikgoz, "Modelling and experimental verification of the operating current of mono-crystalline photovoltaic modules using four- and five-parameter models," *Applied Energy*, Vol. 84, No. 1, pp. 1–15, Jan. 2007.
- [9] Y. C. Kuo, T.-J. Liang, and J.-F. Chen, "Novel maximum-power-point tracking controller for photovoltaic energy conversion system," *IEEE Trans. Ind. Electron.*, Vol. 48, No. 3, pp. 594–601, Jun. 2001.
- [10] Y. Yusof, S. H. Sayid, M. Abdul Latif, and M. Z. C. Wanik, "Modeling and simulation of maximum power point tracker for photovoltaic system," in *Proc. PEC*, pp. 88–93, 2004.
- [11] C. Carrero, J. Amador, and S. Arnaltes, "A single procedure for helping PV designers to select silicon PV module and evaluate the loss resistances," *Renewable Energy*, Vol. 32, No. 15, pp. 2579–2589, Dec. 2007.
- [12] S. Liu and R. A. Dougal, "Dynamic multiphysics model for solar array," *IEEE Trans. Energy Convers.*, Vol. 17, No. 2, pp. 285–294, Jun. 2002.
- [13] S. Yadir, M. Benhmida, M. Sidki, E. Assaid, and M. Khaidar, "New method for extracting the model physical parameters of solar cell using explicit analytic solutions of current-voltage equation," in *Proc. ICM*, pp. 390–393, 2009.
- [14] S. Aazou and E. M. Assaid, "Modeling real photovoltaic solar cell using Maple," in *Proc. ICM*, pp. 394–397, 2009.
- [15] M. G. Villalva, J. R. Gazoli, and E. R. Filho, "Comprehensive approach to modeling and simulation of photovoltaic arrays," *IEEE Trans. Power Electron.*, Vol. 24, No. 5, pp. 1198–1208, May 2009.
- [16] C. Sah, R. N. Noyce, and W. Shockley, "Carrier generation and recombination in  $p$ - $n$  junctions and  $p$ - $n$  junction characteristics," in *Proc. IRE*, Vol. 45, No. 9, pp. 1228–1243, 1957.
- [17] A. Gow and C. D. Manning, "Development of a photovoltaic array model for use in power-electronics simulation studies," *IEE Proc. Elect. Power Appl.*, Vol. 146, No. 2, pp. 193–200, 1999.
- [18] J. A. Gow and C. D. Manning, "Development of a model for photovoltaic arrays suitable for use in simulation studies of solar energy conversion systems," in *Proc. 6th Int. Conf. Power Electron. Variable Speed Drives*, pp. 69–74, 1996.
- [19] S. Chowdhury, G. A. Taylor, S. P. Chowdhury, A. K. Saha, and Y. H. Song, "Modelling, simulation and performance analysis of a PV array in an embedded environment," in *Proc. UPEC*, pp. 781–785, 2007.
- [20] A. Hovinen, "Fitting of the Solar Cell  $I$ - $V$ -curve to the Two Diode Model," *Physica Scripta*, Vol. T54, pp. 175–176, Jun. 1994.
- [21] J. Hyvarinen and J. Karila, "New analysis method for crystalline silicon cells," in *Proc. WCPEC*, Vol. 2, pp. 1521–1524, 2003.
- [22] K. Kurobe and H. Matsunami, "New two-diode model for detailed analysis of multicrystalline silicon solar cells," *Jpn. J. Appl. Phys.*, Vol. 44, pp. 8314–8321, Dec. 2005.
- [23] K. Nishioka, N. Sakitani, K. Kurobe, Y. Yamamoto, Y. Ishikawa, Y. Uraoka, and T. Fuyuki, "Analysis of the temperature characteristics in polycrystalline si solar cells using modified equivalent circuit model," *Jpn. J. Appl. Phys.*, Vol. 42, pp. 7175–7179, Dec. 2003.
- [24] K. Nishioka, N. Sakitani, Y. Uraoka, and T. Fuyuki, "Analysis of multicrystalline silicon solar cells by modified 3-diode equivalent circuit model taking leakage current through periphery into consideration," *Solar Energy Mater. Solar Cells*, Vol. 91, No. 13, pp. 1222–1227, Aug. 2007.
- [25] H. Patel and V. Agarwal, "MATLAB-based modeling to study the effects of partial shading on PV array characteristics," *IEEE Trans. Energy Convers.*, Vol. 23, No. 1, pp. 302–310, Mar. 2008.
- [26] D. Archer and R. Hill, *Clean electricity from photovoltaics, Series on Photoconversion of Solar Energy*, Imperial College Press, pp. 868, Jun. 2001.
- [27] McIntosh KR, Altermatt PP, Heiser G., "Depletion-region recombination in silicon solar cells: when does  $mDR=2$ ?", in *Proc. 16th European Photovoltaic Solar Energy Conf.* pp. 251–254, 2000.
- [28] KC200GT High Efficiency Multicrystal Photovoltaic Module Datasheet Kyocera - <http://www.kyocera.com.sg/products/solar/pdf/kc200gt.pdf>.
- [29] Solarex MSX60 and MSX64 Solar Arrays Datasheet - <http://www.californiasolarcenter.org/newssh/pdfs/solarex-MSX64.pdf>.
- [30] Shell Solar Product Information Sheet.
- [31] Introduction to power electronics course notes, ECEN 2060 - <http://ecee.colorado.edu/ecen2060/matlab.html>, 2008.



**Kashif Ishaque** received his B.E. in Industrial Electronics Engineering from Institute of Industrial Electronics Engineering, NEDUET, Karachi, Pakistan, in 2007, and his M.E. in Mechatronics and Automatic Control in 2009 from the Universiti Teknologi Malaysia (UTM), Malaysia, where he is currently working toward his Ph.D. in Electrical Engineering. He is a lecturer at the PAF Karachi Institute of Economics and Technology (PAF-KIET), Karachi, Pakistan. His research interests include photovoltaic modeling and control, intelligent control, nonlinear systems control and optimization techniques such as genetic algorithm (GA), particle swarm optimization (PSO) and differential evolution (DE).



**Zainal Salam** obtained his B.S., M.E. and Ph.D. from the University of California, the Universiti Teknologi Malaysia (UTM) and the University of Birmingham, UK, in 1985, 1989 and 1997, respectively. He has been a lecturer at UTM for 24 years and is now a Professor of Power Electronics in the School of Electrical Engineering. He has been working on several research and consulting projects in the area of battery powered converters. Currently he is the Director of the Inverter Quality Control Center (IQCC) at UTM which is responsible for testing PV inverters that are to be connected to the local utility grid. His research interests include all areas of power electronics, renewable energy, power electronics and machine control.



**Hamed Taberi** was born in Babol, Iran in 1985. He received his B.S. in Electrical Engineering from the University of Mazandaran, Iran, in 2009. Currently he is working toward his M.E. in Electrical Engineering at the Universiti Teknologi Malaysia (UTM), Malaysia. He is an Assistant in the Inverter Quality Control Center (IQCC) UTM which is responsible for testing PV inverters that are to be connected to the local utility grid. His research interests include the maximum power point tracking control of photovoltaic systems, power systems, power quality, transformers and power electronics.